Waveguide mode in the box with an extraordinary flat dispersion curve

N. Rassem, A.-L. Fehrembach, and E. Popov*

Aix-Marseille Université, CNRS, Centrale Marseille, Institut Fresnel UMR 7249, 13013 Marseille, France
**Corresponding author: e.popov@fresnel.fr*

Received October 29, 2014; revised December 23, 2014; accepted January 9, 2015;
posted January 12, 2015 (Doc. ID 225942); published February 11, 2015

The extraordinary flattening of the dispersion curve of the so-called cavity resonator integrated guided-mode resonance filters (CRIGFs) is analyzed and explained as due to the intramode coupling imposed by the external Bragg resonators. CRIGFs are composed of a grating coupler (guided-mode resonance filter, GMRF) put between two distributed Bragg reflectors (DBRs). They form a cavity box in which the excited guided mode is confined. This confinement provides resonances with small spectral width (smaller than 1 nm for optical wavelengths) and extraordinary wide angular acceptance (several degrees). At a first glance, one may think that similar performances could be obtained while putting the GMRF and the DBR one above the other, forming a so-called "doubly periodic" grating, as in this configuration also the DBR confines the mode. Yet, the angular acceptance of CRIGFs is an order of magnitude greater than in classical gratings, even with complex pattern. The aim of the present paper is to identify the phenomenon responsible for the extraordinary large angular acceptance of CRIGFs. We numerically calculate, for the first time to the best of our knowledge, the dispersion curve of the mode excited in the CRIGF. The dispersion curve shows a flat part, where the resonance wavelength is quasi-independent of the angle of incidence, and the flattening grows with the width of the Bragg reflector. We develop an approximate coupled four-wave model, which predicts the extraordinary flattening as a consequence of an additional coupling of the waveguide modes of the GMRF provided by the Bragg grating, that does not exist in the "doubly periodic" gratings.

OCIS codes: (050.2770) Gratings; (050.6624) Subwavelength structures; (230.1480) Bragg reflectors; (050.5745) Resonance domain; (230.7408) Wavelength filtering devices.
http://dx.doi.org/10.1364/JOSAA.32.000420

1. INTRODUCTION

Narrowband filters are key components in fields such as optical telecommunications and spectroscopy. Guided-mode resonance gratings are promising structures that could bring a breakthrough in narrowband filtering. They are composed of a stack of dielectric layers, playing the role of a planar waveguide, engraved with a subwavelength grating. Depending on the incident wave, one eigenmode of the structure can be excited through one diffraction order of the grating that acts as a grating coupler [1,2]. This results in a resonance peak in the reflection or transmission spectrum of the component. The major advantage of this peak is its thinness, which can be theoretically as tiny as desired, depending on the perturbation caused by the grating. A record experimental 0.03 nm bandwidth at 560 nm has been reported [3].

Another property of resonant grating filters is their strong dependence on the polar angle of incidence. This property can be used to tune the centering wavelength of the filter with respect to the angle of incidence [4]. Such a component can find application in spectroscopic imaging. However, the strong angular dependency is undoubtedly a drawback for applications in which large parallel incident beams cannot be used, either due to limitations on the beam collimation or on the size of the grating. Indeed, the resonance peak crushes if the divergence of the incident beam is not small enough as compared to the angular acceptance of the filter [5–7]. Moreover, experimental works have shown that the quality factor of the resonance is very sensitive to etching imperfections all over the grating surface [8,9]. A component with a high angular acceptance could be illuminated with a focused beam, thus limiting the impact of etching imperfections.

The angular acceptance can be enhanced by flattening of the mode dispersion curve by working at the boundaries of the forbidden zone formed due to the mode interactions inside the grating. This can be done typically by using a Bragg grating that concentrates the stationary mode generated by the excitation of two counter-propagative modes. The Bragg grating and the grating coupler can be merged leading to a grating with a complex basic pattern called "doubly periodic" [10]. The 1D (periodic along one direction) "doubly periodic" pattern is composed of two grooves with different sizes, and the 2D (periodic along two directions) "doubly periodic" pattern is composed of four holes with different diameters. In 2010, a bandwidth of 0.28 nm at 1550 nm was experimentally measured in a 2D "doubly periodic" grating illuminated with a Gaussian beam having a 200 μm diameter at the waist [8].

The major drawback of the "doubly periodic" pattern is that the angular acceptance and the spectral bandwidth cannot be tuned independently: the maximum bounding of the mode comes with an infinitely narrow spectral peak. To overcome this problem, the Bragg grating and the grating coupler must be pulled apart, either vertically or horizontally. In the first case, the component is still a grating (theoretically infinite), and its properties are well understood thanks to the large amount of theoretical work on guided-mode resonance filters (GMRFs) reported in the literature [11–13]. The second case

corresponds to a finite structure that was first suggested in 2008 for surface-normal emission [14,15], and is now known as a cavity resonator integrated guided-mode resonance filter (CRIGF). The predicted performances are bandwidths smaller than 0.7 nm in the near infrared for components with aperture size less than 10 μm in diameter [16,17], which is 20 times smaller than what can be expected with a "doubly periodic" pattern grating. A polarization-independent filter was also experimentally demonstrated using a 2D pattern [18]. Two recent papers present the interest of CRIGF for the field of lasers [19,20].

Because of their long (with respect to the wavelength) but finite size, and their subwavelength patterning, numerical modeling of CRIGFs is time consuming. In order to design components, approximate models based on the coupled-mode theory were developed [14,16]. Yet, to the best of our knowledge, no tentative explanation of the physical origin of the spectacular wide angular acceptance of CRIGFs has been reported. In the present paper, our purpose is to propose a simple physical explanation of the functioning of CRIGFs based on the additional coupling (provided by the Bragg gratings) between the initial four modes supported by the grating coupler near normal incidence, a coupling that leads to a super-flattening of the mode dispersion curves and thus to large angular tolerances.

Our paper is organized as follows: we first present numerical results using rigorous electromagnetic modeling emphasizing the difference in the angular behavior of CRIGFs and classical gratings. Then, we switch to the homogeneous problem by calculating a dispersion relation of the excited mode. For this, we use two different complimentary electromagnetic approaches that permit working either with complex wavelength or complex angle of incidence values. Last, we present an approximate model, combining the coupled-mode theory applied to four modes and the transmission matrix method, to explain the physical origin of the flattening of the dispersion curve of CRIGFs.

2. REFLECTION PROPERTIES OF TWO TYPES OF RESONANT GRATING FILTERS

Figure 1(a) shows the schematic view of the CRIGF under study: this structure is composed of one GMRF section (21 periods) and two distributed Bragg reflector (DBR) sections (N_{DBR} periods). We also define a phase section ($\delta = 1.05d$) that is inserted between the GMRF and the Bragg reflectors. The GMRF and the Bragg sections have both a groove width $a = 100$ nm and depth $h_1 = 120$ nm. The guiding layer thickness is $h_2 = 165$ nm. The indices of the materials are 1.46 for the gratings and 1.97 for the guiding layer. The superstrate is air with index 1.0 (the same for the grating grooves), and the substrate is silica with index 1.46. The period of the central section is $d = 532$ nm. The so-called "doubly periodic" structure is represented in Fig. 1(b). It is composed of the same guiding layer, GMRF, and Bragg gratings as the CRIGF of Fig. 1(a), except that the GMRF and Bragg gratings are located one above the other, thus forming an infinite (periodic) structure. The values of the parameters are the same as that of the CRIGF [Fig. 1(a)]. The numerical modeling introduces a periodicity of the system in x direction having as a super-period the entire CRIGF length. In order to avoid the coupling between the different super-periods [Fig. 1(c)], we introduce absorbing regions between them, as explained in detail at the end of this section.

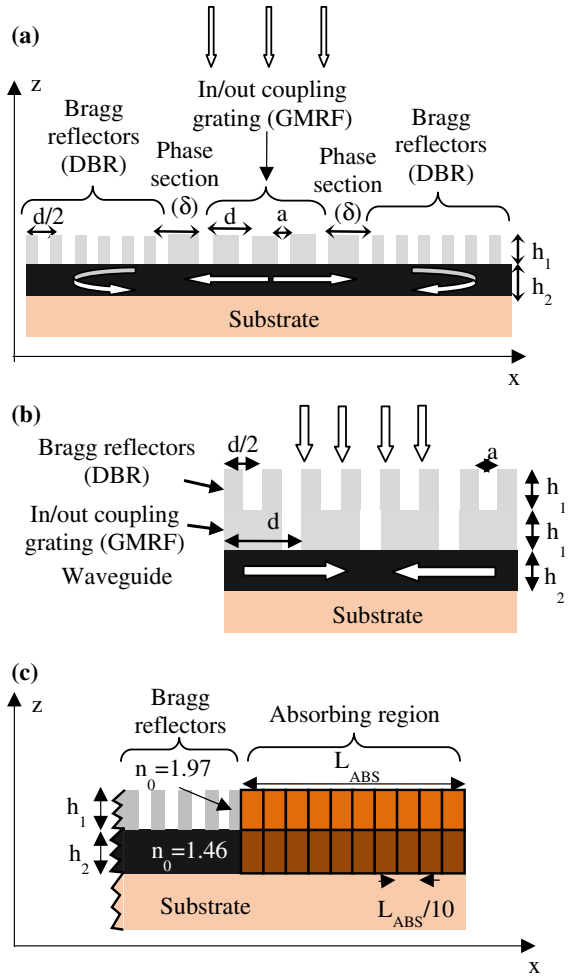

Fig. 1. Schematic view of (a) the CRIGF, (b) the "doubly periodic" grating studied, with period of the GMRF d, period of the Bragg grating d/2, width of the grooves a, gratings depth h_1, guiding layer thickness h_2, phase section length δ (for the CRIGF only), and (c) the additional absorbing layers between the supercells during the numerical modeling.

In Fig. 2, we plot the reflectivity of the CRIGF and of the "doubly periodic" grating when varying the radius at the waist of the incident Gaussian beam. We observe in Fig. 2(a) that for a radius value around 5.7 μm the peak is maximal, while it widens and its maximum value reduces for greater or smaller radii. The width of the GMRF section is around 11 μm; hence, the optimum (peak maximum around 85%) is obtained when the beam spot recovers almost completely the GMRF area. For larger beams, the beam spreads over the Bragg grating area; thus a part of the beam cannot be coupled into the guided mode. For smaller beams, the divergence of the beam becomes greater than the angular acceptance of the filter. The behavior of the "doubly periodic" grating is very different [see Fig. 2(b)]. For large beams (waist greater than 100 μm), the peak reaches 100%, same as that obtained when the component is illuminated with a plane wave. When the waist decreases, we observe the widening and decreasing of the resonance peak. For both structures, the case for $\omega_0 = 12$ μm is represented, showing the interest of CRIGFs compared to

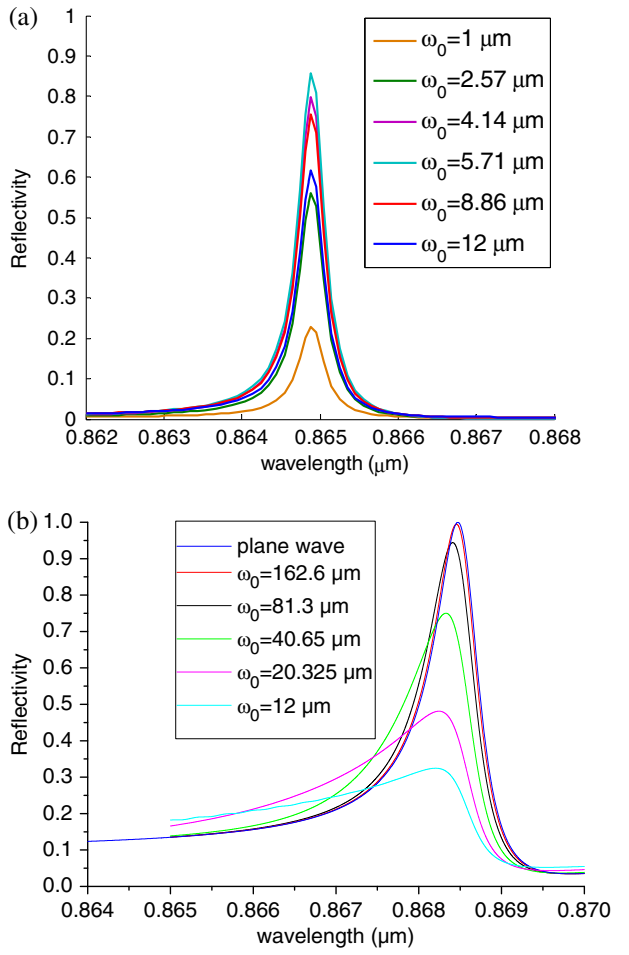

Fig. 2. Reflectivity spectra for Gaussian beams with different radii ω_0 at the waist under normal incidence for (a) the CRIGF and (b) the "doubly periodic" grating.

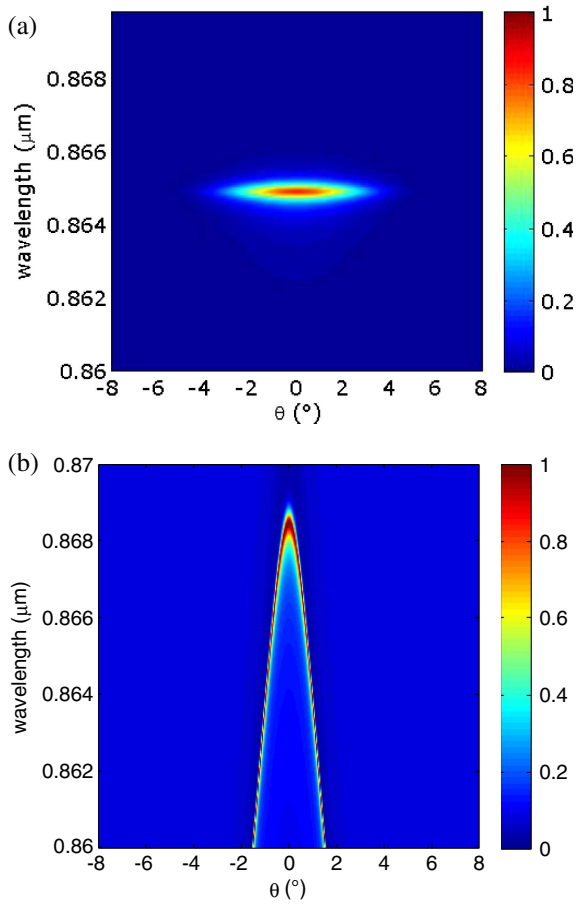

Fig. 3. Reflectivity in the specular beam as a function of the polar angle of incidence θ ($\theta = 0°$ under normal incidence) and of the wavelength λ, for (a) the CRIGF illuminated with a Gaussian beam (radius at waist = 5.2 μm) and (b) the "doubly periodic" grating illuminated with a plane wave.

"doubly periodic" pattern gratings when illuminated with a focused beam.

The reflectivity versus the wavelength λ and the polar angle of incidence θ is plotted for the CRIGF [Fig. 3(a)] and the "doubly periodic" grating [Fig. 3(b)]. The maps are very different: for the infinite grating [Fig. 3(b)], the $R(\theta, \lambda)$ map shows the well-known forbidden band, with the lower branch of the dispersion curve only represented here, a gap that appears due to the simultaneous excitation, under normal incidence, of two counter-propagative modes; for the CRIGF, we observe a horizontal spot where the reflectivity is maximum. The spot is centered at $\lambda = 864.9$ nm and normal incidence. When the angle of incidence increases (in absolute value), or the wavelength moves away from 864.9 nm, the reflected energy decreases: the resonance degrades. This device has a wide angular acceptance, from −2° to 2°, together with a thin spectral width. The results of the calculations presented here were obtained using the Fourier modal method [21], also known as the rigorous coupled wave (RCW) method [22], improved by using the more rapidly converging rules of factorization of the product of discontinuous functions [23,24]. The number of Fourier harmonics is truncated to from −700 to 700. In order to avoid parasite coupling between the field in the different super-periods, absorbing regions of length $L_{ABS} = 2.66$ μm are included at each side of the structure inside the grating and guiding layers [having thicknesses h_1 and h_2, respectively, in Fig. 1(a)]. The absorbing regions are formed by using ten homogeneous rectangular rods in each layer [see Fig. 1(c)]. The refractive index n_p of the p-th rod is calculated as $n_p = n_0 + i(p/10)^2$ for p, an integer varying from 1 to 10, so that the imaginary part of the refractive index increases from zero to one from the beginning to the end of the absorbing region. The starting value n_0 is that of the material of the layer of the structure immediately adjacent to the absorbing region [see Fig. 1(c)].

3. HOMOGENEOUS PROBLEM

In order to better understand the physical origin of the different behavior of the reflectivity of the two systems, it is necessary to study the dispersion relations of their resonances. Since the working region lies close to the gap boundaries, it is not sufficient to only represent the response for real values of wavelength and angle of incidence, as it is done in Fig. 3. Much more information can be obtained by solving the homogeneous problem for complex values of the wavelength λ and/or propagation constant γ along x. To calculate the dispersion relation of the CRIGF, we used two different methods: first the search of the poles of the scattering matrix, and second the search of the eigenvalues of the transmission matrix, as explained below.

The resonances in the grating coupler are characterized by complex values of the pole of the scattering matrix, due to coupling with the propagating incident wave (radiation losses), but also due to the formation of a forbidden gap due to the interaction between counter-propagating waveguide modes [25]. The results of the numerical search of the poles λ_p of the CRIGF system in the complex λ plane are presented in Fig. 4, with the real part of the pole (λ_p) given in Fig. 4(a), and the imaginary part in Fig. 4(b). These curves show a weak dependence versus the angle of incidence for $\theta < 2°$. In this angular interval, the spectral position of the pole is practically independent of the angle of incidence, a fact that confirms the $R(\theta, \lambda)$ map: the real part is around 864.9 nm, and the imaginary part stays constant. When θ becomes greater than 2°, the real part of λ decreases rapidly, and one observes a sharp increase in the imaginary part, which goes with the degradation of the resonance peak value. This study links the reflectivity of the system with the behavior of the resonance, but it cannot explain why the pole behaves like this, i.e., what is the physical reason of the origin of the flat part.

In order to search for such explanation, we shall try to study the system properties, in particular, its resonances, by varying the strength (length) of the Bragg grating mirrors. For this, we use another approach, proposed by Cao *et al.* [26], consisting of studying the modes of the system by considering it finite in the horizontal (x) direction and periodizing it in the vertical (z) direction. This requires introducing absorbing regions between the different periods in the vertical (z) direction, in the same manner as explained previously at the end of the previous section. Here the total length of the absorbing regions is $L_{ABS} = 2.51$ μm.

There are two advantages of this approach. First, the system period in the vertical direction can be much shorter than the horizontal length in the configuration presented in Fig. 1. For example, it is sufficient to introduce a vertical period of 14 μm, which requires ten times less Fourier components (from −70 to 70) to obtain converging results. Second, the system resonance values (complex propagation constants) are obtained by a single calculation of the eigenvalues of the transmission matrix [as explained in Appendix A, Eqs. (A23)–(A25)], instead of making a search of the poles of the scattering matrix in the complex plane. The eigenvalues χ of each mode represent the phase shift and the decay of the field of the mode when it propagates inside the structure in the x direction with propagation constant $\gamma : \chi = \exp(i\gamma L)$, where L is the length of the structure (in the x direction).

However, there is a price to pay: the eigenvalues correspond to all the resonances of the system, not only to the ones that are searched as considered being the interesting ones. As an illustration, Fig. 5 presents the spectral dependence of the imaginary part of the propagation constant γ of the modes of the structure of Fig. 1(a) for $N_{DBR} = 200$. One can see many different propagation constants with imaginary parts that depend quasi-linearly on the wavelength and correspond to quasi-plane waves that can propagate in the substrate or in the cladding because their total thickness is about 10 μm. Among the values represented in Fig. 5, two sets have a different behavior, showing an imaginary part that draws three major foils as a function of the wavelength, resembling the behavior in the imaginary part of the mode dispersion curves inside the forbidden gap. This mode presents a particular interest because it is strongly affected by the Bragg grating (for example, see Fig. 8), and in the following we shall focus on it. The technical problem consists of identifying its real part, which has to be done manually.

We plot in Fig. 6 its real part that is characterized by a flat portion that appears around 864.9 nm, which corresponds to the center wavelength of the peak observed in Fig. 3(a). Note that the real part of the propagation constant is defined with an indetermination of $2\pi/L = 0.0529$ μm^{-1}, with L being the total length of the structure (L = 118.6892 μm). Hence, no

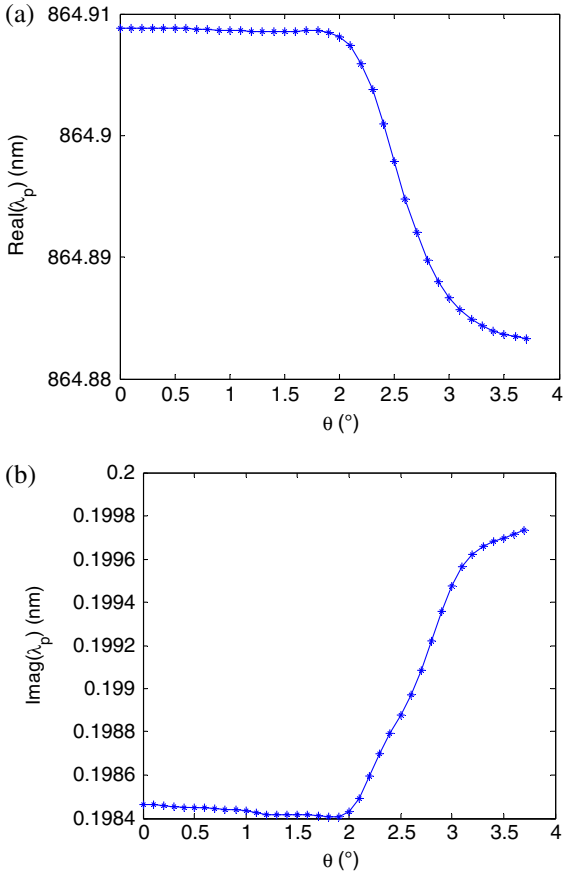

Fig. 4. (a) Real and (b) imaginary parts of the pole for the CRIGF, versus the incidence angle (θ).

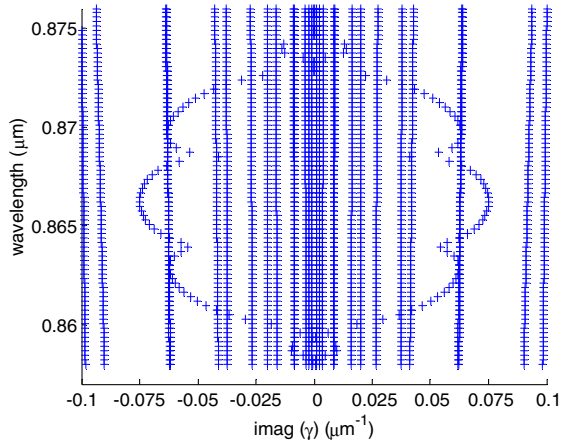

Fig. 5. Spectral dependence of the imaginary part of the eigenvalues of the CRIGF of Fig. 1(a) for $N_{DBR} = 200$.

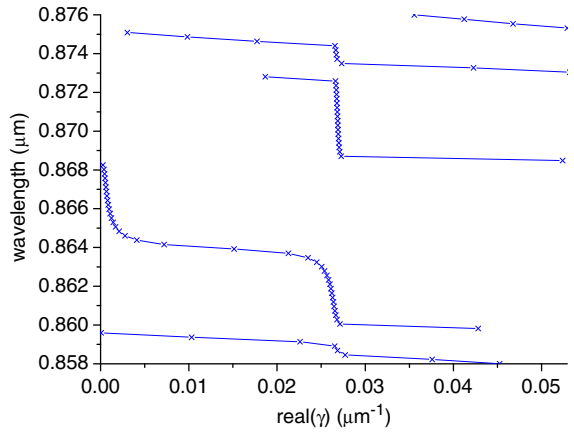

Fig. 6. Real part of the interesting eigenvalue extracted.

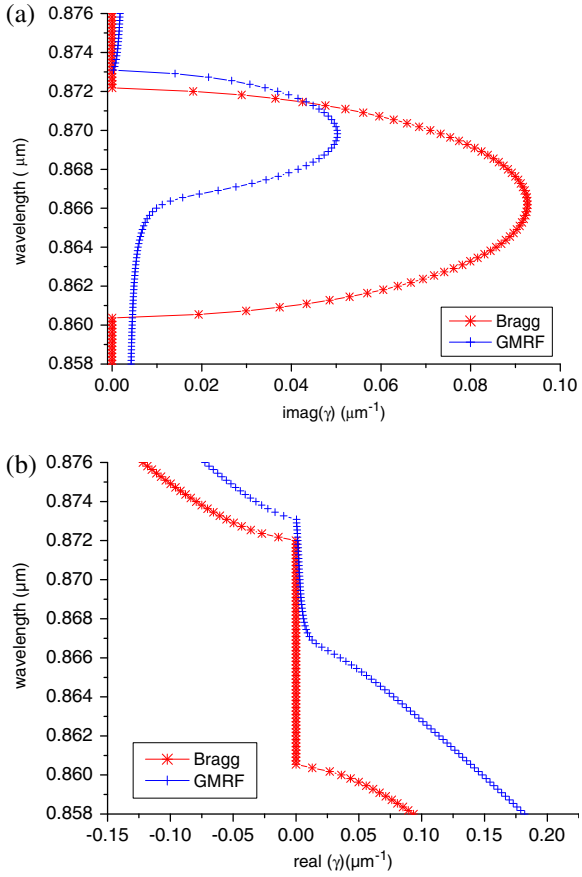

Fig. 7. Bragg (stars) and GMRF (crosses) forbidden bands from the calculation of the eigenvalues. (a) Real and (b) imaginary parts with respect to the wavelength.

further conclusion can be drawn for the value of the real part of the propagation constant outside this region [−0.0529/2; 0.0529/2 μm^{-1}], yet another disadvantage of this approach.

4. EXPLANATION OF THE ORIGIN OF THE SUPER-FLATTENING OF THE BAND EDGE OF CRIGFS

The dispersion relation of the modes of the CRIGF has to be compared with that of the modes of the finite-size GMRF [central grating in Fig. 1(a)] and of the Bragg grating. Figure 7 shows the Bragg (stars) and GMRF (crosses) bandgap formed by the propagation constant calculated from the eigenvalues. The GMRF bandgap is quasi-included in the Bragg bandgap, as it must be, as far as the Bragg grating serves for a distributed mirror. The forbidden band of the Bragg grating is located between 860.5 and 872.2 nm and is symmetric with respect to 866 nm. The GMRF forbidden band is asymmetric: on the lower edge of the gap, the imaginary part is non-null; it is related to the leakage of the mode in the superstrate and the substrate. It is well known that at the edges of the bandgap, a symmetric and an antisymmetric mode appear. The symmetric mode can couple to the (symmetric) propagative plane wave while it is not the case for the antisymmetric mode. Thus, we can guess from Fig. 7 that the symmetric mode is located at the lower edge, as the imaginary part of its propagation constant is non-null due to the possible coupling with the incident wave. On the other hand, the antisymmetric mode is located at the upper edge, its imaginary part is zero and it cannot interact with the incident wave under normal incidence. The two gratings periods have been chosen so that the wavelength of the symmetric mode is located in the middle of the gap of the Bragg grating.

As already said, we are interested in the evolution of the dispersion relations (the real and the imaginary part of γ) when introducing different strengths of the Bragg reflectors, by varying the number N_{DBR} of grooves of the Bragg grating. The central grating length is fixed constant, so that when varying the Bragg grating length, the length L_{DBR} of the whole structure with N_{DBR} Bragg periods at each side of the GMRF varies. Figure 8 presents the evolution of the "good" propagation constant when the value of the Bragg periods number (N_{DBR}) increases from 1 to 200. As far as the values of real(γ) are determined within integer times $2\pi/L_{DBR}$, in order to avoid the change in this ambiguity, we plot real(γ)L_{DBR}/L with respect to the wavelength, where the total normalization length L = 118.6892 μm is kept fixed. We observe that the shape of the real part changes gradually with the DBR groove numbers, starting from the single-grating curve (Fig. 7) toward the curve given in Fig. 6. An increasingly flatter region is formed in the wavelength interval 0.865–0.869 μm.

The conclusion of this study is that the Bragg grating reflection plays a decisive role in the formation of the flat part in the dispersion curve, where the stronger the coupling, the flatter the curve. A natural question rises with respect to this

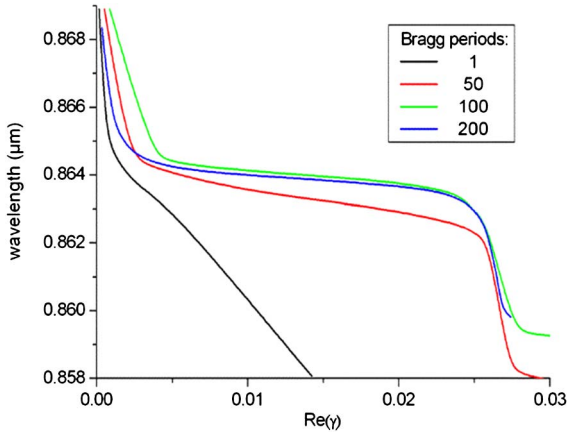

Fig. 8. Evolution of the real part of the eigenvalues for different values of N_{DBR} (1, 50, 100, 200).

phenomenon: why it has not been observed in the almost half-century development of integrated optics. The answer is that in integrated optics, the main interest is in manipulating the propagating modes, i.e., when the Bragg distributed mirrors are used to deflect waveguides modes that are far from the forbidden gap boundaries. In our case the situation is completely different, the modes of the central CRIGF region are close to the forbidden gap boundary, in order to initially flatten the dispersion curves by using the contra-propagative mode coupling. As it is well-known (see Appendix A), this coupling leads to a formation of two hybrid standing modes with slightly different constants of propagation k^+ and k^- (Eq. A3), separated by twice their distance from the gap boundary. When this separation is large (small contra-propagating coupling), their mutual conversion on the Bragg mirror is negligible. However, when their difference is small (close to the gap edge), these two waves can be mutually coupled.

In order to directly study the role of this additional coupling, we have developed an approximate four-wave coupled-mode model, as described in Appendix A. The approach takes into account the coupling due to the Bragg grating of the four waves (two with propagation constant k^+ propagating in opposite directions and two with propagation constant k^-). We consider two different coupling processes: the Bragg reflection into the same mode (k^+ to $-k^+$ or k^- to $-k^-$, as has been usually done up to now) and the coupling between the different modes of the central section (k^+ to $-k^-$, for example). The strength of the latter coupling can become large due to the fact that the modal structure of the Bragg grating and the central CRIGF, when considered separately, are quite different, as can be judged from the difference in the propagation constants of the initial modes, as given in Fig. 7. This difference results in non-null overlapping integrals R^{-+} and R^{+-} (Eq. A14). The real part of the calculated propagation constant with respect to the wavelength is plotted in Fig. 9 for different values of the overlapping integral, in the case $R^{-+} = R^{+-}$. It is obvious that the additional coupling leads to an additional flattening of the dispersion curve. In order to take into account that the effective propagating length of the modes of the central section is greater than its length, due to the partial penetration in the Bragg gratings, we have taken in the approximate calculations a GMRF twice longer than in the previous rigorous calculations ($L = 2 \times 12.2892$ μm). Only a zoom close to the lower gap boundary is given. The initial mode of CRIGF is supposed to have a constant of propagation $k_g = k_0(1.636 + i0.0001)$ and the contra-propagation coupling coefficient $\kappa = 0.01k_0^4/k_g^2$. The initial mode of the Bragg grating has the parameters $k_{B,g} = k_0(1.63 + i0)$ and $\kappa = 0.0225k_0^4/k_{B,g}^2$. The parameters are adjusted to correspond to the results in Fig. 6. As explained in Appendix A, we neglect the losses due to the transition phenomena on the interface between the central region and the Bragg gratings. As observed in Fig. 9, if the intermodal conversion is neglected ($R^{+-} = 0$), the real part of γ has the same behavior as in Fig. 8 without the Bragg reflector. As R^{+-} increases, the curve flattens, and the gap boundary is blueshifted. At its maximum ($R^{+-} = R^{++} = \sqrt{0.5}$), the curve has an almost flat region, as was true for the maximum length of the Bragg gratings in Figs. 7 and 8.

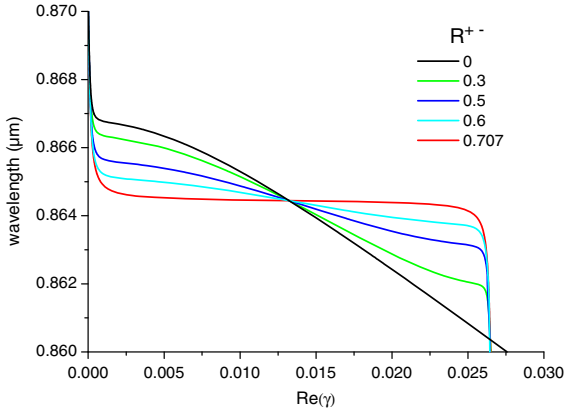

Fig. 9. Evolution of the real part of the eigenmodes propagation constant as a function of the factor of conversion between the hybrid modes of CRIGF due to the Bragg mirror reflection, as calculated using the approximate four-wave coupled theory developed in Appendix A.

5. CONCLUSION

In order to investigate the physical origin of the extraordinary angular tolerance of CRIGFs, we adopt an original approach based on the resolution of the homogeneous problem (search for the eigenfrequencies of the mode in the complex plane). Numerically, we showed that the flattening of the dispersion curve increases as the strength of the Bragg reflection rises up with the growing number of Bragg periods. This behavior is reproduced with the approximate model we developed based on the four-mode coupled-mode theory. As it is well-known from the two-wave coupled-mode theory, the interaction between two counter-propagative modes leads to the creation of two hybrid modes, one with a larger (k^+) and the other with a smaller (k^-) constant of propagation. The Bragg grating cavity resonator that contains the central GMRF grating can lead to a well-known reflection of the mode "k+" into the mode "−k+" (and similarly for k^-), but also can provide an additional coupling between the hybrid modes ("k+" into "−k−") that does not exist without the Bragg grating box. We have shown that the strength of this additional coupling (proportional to overlapping integral R^{-+}) is directly responsible for the flattening of the dispersion curve of the mode of the entire system. In particular, when the two types of coupling have similar strengths, one observes an extraordinary flattening of the dispersion curve of CRIGF devices. The performance of the device can be critical for some applications that cannot afford substantial beam collimation that is necessary for classical grating filters, or for applications that *a priori* need focused light beams, as it is, for example, in confocal microscopy.

An interesting extension of these studies can be considered by using two-dimensional periodic structures aiming to efficient filtering in unpolarized light. Promising experimental techniques have already been proposed [18,27,28] in the literature. However, this is one of the rare cases when the numerical modeling could be more difficult to perform than the experimental realization because of the large device dimensions with respect to the wavelength.

APPENDIX A: FOUR-MODE COUPLED-MODE THEORY

1. Eigenmodes at the Band Edge for an Infinite Grating

Let us consider a grating waveguide, invariant in the y direction, that supports leaky modes propagating in the x direction,

with leakage κ_{out} due to the radiation into propagating diffraction orders in the substrate and the superstrate. The vector field components of the mode F(x, z) can be factorized in the form

$$F(x,z) = f(z)e^{ik_g x}. \tag{A1}$$

The propagation constant k_g is real without grating for waveguides made of lossless materials. For a grating waveguide, the radiation losses enter in the mode propagation constant along x and increase its imaginary part,

$$k_g = Re(k_g) + i(\kappa_{out} + \kappa_{a.l.}), \tag{A2}$$

with $\kappa_{a.l.}$ staying for the absorption losses, if any.

In addition to the leakage, the mode propagation constant and field map can be modified by the interaction between counter-propagating modes. The classical coupled-mode theory shows that this coupling modifies the propagation constant and forms a forbidden gap in its dispersion map, the modification resulting in a formation of two hybrid modes having two slightly different propagation constants:

$$k^+ = K + \Delta, k^- = K - \Delta, \tag{A3}$$

with

$$\Delta = \sqrt{(K - k_g)^2 - \kappa^2}, \tag{A4}$$

where κ is the coupling strength between the two counter-propagating modes and is proportional to the overlap mode integral in the transverse direction. In particular, if the interaction involves the same counter-propagating modes and is due to the grating that extends from 0 to h in the z direction, then

$$\kappa = \frac{\kappa_{-2}\kappa_{+2}}{4k_g^2}, \kappa_{\pm 2} = k_0^2 \int_0^h F_{\pm 2}^T[n^2(x,z)]|f(z)|^2 dz, \tag{A5}$$

and $F_m^T[n^2(x,z)]$ stays for the m-th Fourier transform, along x, of the square of the refractive index function of the grating.

The spectral region in which $|K - k_g| < \kappa$ is forbidden (bandgap) in the sense that the imaginary part of the propagation constant increases due to the backward scattering. At its boundaries, the real part of $k^{\pm}$ has the weakest dependence on the incident vector component, parallel to the surface, and thus the angular tolerances of the filter response are less tight.

2. Transmission Matrix of a CRIGF

Let us consider the CRIGF that consists of a grating that acts to couple in and out the waveguide mode(s) to the incident and reflected waves, and two Bragg reflectors at the two sides of the middle grating. Inside the middle grating, the two hybrid modes, with propagation constants k^+ and k^-, do not interact. However, when entering the Bragg grating region in its gap, there may occur an energy transfer between these two hybrid modes because the field maps of the local modes in the middle grating and in the Bragg gratings can differ significantly, as far as the Bragg gratings act inside their gap.

A simplified model can take into account this interaction, at least approximately, contributing to a better understanding of the underlying phenomenon. Let us consider a TE (transverse electric) mode with an electric field component parallel to the y axis.

If we take into account that in each region we have two possible directions of propagation, the tangential non-null field components can be expressed in the form

$$\begin{pmatrix} E_y^+ \\ i\omega\mu_0 H_z^+ \\ E_y^- \\ i\omega\mu_0 H_z^- \end{pmatrix} = \begin{pmatrix} 1 & 1 & 0 & 0 \\ k^+ & -k^+ & 0 & 0 \\ 0 & 0 & 1 & 1 \\ 0 & 0 & k^- & -k^- \end{pmatrix} \times \begin{pmatrix} e^{ik^+x} & 0 & 0 & 0 \\ 0 & e^{-ik^+x} & 0 & 0 \\ 0 & 0 & e^{ik^-x} & 0 \\ 0 & 0 & 0 & e^{-ik^-x} \end{pmatrix} \begin{pmatrix} a_p^+ \\ a_n^+ \\ a_p^- \\ a_n^- \end{pmatrix}, \tag{A6}$$

with subscripts p and n indicating the positive and negative directions of propagation along the x axis. The transmission matrix inside the middle grating layer having length L is simply given by the expression

$$T = \begin{pmatrix} 1 & 1 & 0 & 0 \\ k^+ & -k^+ & 0 & 0 \\ 0 & 0 & 1 & 1 \\ 0 & 0 & k^- & -k^- \end{pmatrix} \times \begin{pmatrix} e^{ik^+x} & 0 & 0 & 0 \\ 0 & e^{-ik^+x} & 0 & 0 \\ 0 & 0 & e^{ik^-x} & 0 \\ 0 & 0 & 0 & e^{-ik^-x} \end{pmatrix} \begin{pmatrix} 1 & 1 & 0 & 0 \\ k^+ & -k^+ & 0 & 0 \\ 0 & 0 & 1 & 1 \\ 0 & 0 & k^- & -k^- \end{pmatrix}^{-1}. \tag{A7}$$

At the interface between the Bragg and the middle gratings, it is necessary to preserve the continuity of the tangential electric and magnetic field components, namely, E_y and H_z. Assuming the hypothesis that in each of the gratings it is sufficient to consider only the two hybrid modes, the boundary conditions require that

$$\begin{pmatrix} E_{By}^+ + E_{By}^- \\ H_{Bz}^+ + H_{Bz}^- \end{pmatrix} = \begin{pmatrix} E_{Gy}^+ + E_{Gy}^- \\ H_{Gz}^+ + H_{Gz}^- \end{pmatrix}, \quad \text{at} \quad x = 0 \quad \text{or} \quad L, \tag{A8}$$

where B stands for the Bragg grating, G stands for the middle grating, and + and − correspond to the two different constants, as given in Eq. (A3). It must be pointed out that their values are different in each grating.

Let us underline that each of the field components represent a single mode, giving the possibility to separate the variables by use of transverse field distributions f(z), such that

$$E^{+,-}_{B,Gy}(x,z) = f^{+,-}_{B,G}(z)\mathbb{E}^{+,-}_{B,Gy}(x),$$
$$H^{+,-}_{B,Gz}(x,z) = f^{+,-}_{B,G}(z)\mathbb{H}^{+,-}_{B,Gz}(x). \quad \text{(A9)}$$

They are normalized so that the transverse field integral is equal to one:

$$\int_{-\infty}^{+\infty} |f(z)|^2 dz = 1. \quad \text{(A10)}$$

Thus,

$$\begin{pmatrix} E^{+}_{Gy} + E^{-}_{Gy} \\ H^{+}_{Gz} + H^{-}_{Gz} \end{pmatrix}_{x=0} = \begin{pmatrix} f^{+}_{G}(z) & 0 & f^{-}_{G}(z) & 0 \\ 0 & f^{+}_{G}(z) & 0 & f^{-}_{G}(z) \end{pmatrix} \begin{pmatrix} \mathbb{E}^{+}_{Gy} \\ \mathbb{H}^{+}_{Gz} \\ \mathbb{E}^{-}_{Gy} \\ \mathbb{H}^{-}_{Gz} \end{pmatrix}_{x=0}, \quad \text{(A11)}$$

and a similar expression is valid inside the Bragg-grating region. Then Eq. (A8) applied at $x = 0$ takes the form

$$\begin{pmatrix} f^{+}_{G}(z) & 0 & f^{-}_{G}(z) & 0 \\ 0 & f^{+}_{G}(z) & 0 & f^{-}_{G}(z) \end{pmatrix} \begin{pmatrix} \mathbb{E}^{+}_{Gy} \\ \mathbb{H}^{+}_{Gz} \\ \mathbb{E}^{-}_{Gy} \\ \mathbb{H}^{-}_{Gz} \end{pmatrix}_{x=0} = \begin{pmatrix} f^{+}_{B}(z) & 0 & f^{-}_{B}(z) & 0 \\ 0 & f^{+}_{B}(z) & 0 & f^{-}_{B}(z) \end{pmatrix} \begin{pmatrix} \mathbb{E}^{+}_{By} \\ \mathbb{H}^{+}_{Bz} \\ \mathbb{E}^{-}_{By} \\ \mathbb{H}^{-}_{Bz} \end{pmatrix}_{x=0}. \quad \text{(A12)}$$

Because the two hybrid modes are mutually independent in each grating region, we can use the orthogonality between f^{+}_{G} and f^{-}_{G}. First, we multiply by $\bar{f}^{+}_{G}$ (overbar means complex conjugated) and integrate in z:

$$\begin{pmatrix} 1 & 0 & 0 & 0 \\ 0 & 1 & 0 & 0 \end{pmatrix} \begin{pmatrix} \mathbb{E}^{+}_{Gy} \\ \mathbb{H}^{+}_{Gz} \\ \mathbb{E}^{-}_{Gy} \\ \mathbb{H}^{-}_{Gz} \end{pmatrix} = \begin{pmatrix} R^{++} & 0 & R^{-+} & 0 \\ 0 & R^{++} & 0 & R^{-+} \end{pmatrix} \begin{pmatrix} \mathbb{E}^{+}_{By} \\ \mathbb{H}^{+}_{Bz} \\ \mathbb{E}^{-}_{By} \\ \mathbb{H}^{-}_{Bz} \end{pmatrix}, \quad \text{(A13)}$$

with

$$R^{++} = \int_{-\infty}^{+\infty} f^{+}_{B}\bar{f}^{+}_{G} dz,$$
$$R^{-+} = \int_{-\infty}^{+\infty} f^{-}_{B}\bar{f}^{+}_{G} dz. \quad \text{(A14)}$$

Second, Eq. (A12) is multiplied by $\bar{f}^{-}_{G}$ and integrated in z:

$$\begin{pmatrix} 0 & 0 & 1 & 0 \\ 0 & 0 & 0 & 1 \end{pmatrix} \begin{pmatrix} \mathbb{E}^{+}_{Gy} \\ \mathbb{H}^{+}_{Gz} \\ \mathbb{E}^{-}_{Gy} \\ \mathbb{H}^{-}_{Gz} \end{pmatrix}_{x=0} = \begin{pmatrix} R^{+-} & 0 & R^{--} & 0 \\ 0 & R^{+-} & 0 & R^{--} \end{pmatrix} \begin{pmatrix} \mathbb{E}^{+}_{By} \\ \mathbb{H}^{+}_{Bz} \\ \mathbb{E}^{-}_{By} \\ \mathbb{H}^{-}_{Bz} \end{pmatrix}_{x=0}. \quad \text{(A15)}$$

Combining Eqs. (A13) and (A15) together, one obtains that

$$\begin{pmatrix} \mathbb{E}^{+}_{Gy} \\ \mathbb{H}^{+}_{Gz} \\ \mathbb{E}^{-}_{Gy} \\ \mathbb{H}^{-}_{Gz} \end{pmatrix}_{x=0} = \begin{pmatrix} R^{++} & 0 & R^{-+} & 0 \\ 0 & R^{++} & 0 & R^{-+} \\ R^{+-} & 0 & R^{--} & 0 \\ 0 & R^{+-} & 0 & R^{--} \end{pmatrix} \begin{pmatrix} \mathbb{E}^{+}_{By} \\ \mathbb{H}^{+}_{Bz} \\ \mathbb{E}^{-}_{By} \\ \mathbb{H}^{-}_{Bz} \end{pmatrix}_{x=0}. \quad \text{(A16)}$$

Let us denote with R the matrix that contains the overlap integrals. The transmission through the first Bragg grating from $x = -L_B$ to $x = 0$ is expressed through the corresponding transmission matrix T_B, so that

$$\begin{pmatrix} \mathbb{E}^{+}_{Gy} \\ \mathbb{H}^{+}_{Gz} \\ \mathbb{E}^{-}_{Gy} \\ \mathbb{H}^{-}_{Gz} \end{pmatrix}_{x=0} = R \begin{pmatrix} \mathbb{E}^{+}_{By} \\ \mathbb{H}^{+}_{Bz} \\ \mathbb{E}^{-}_{By} \\ \mathbb{H}^{-}_{Bz} \end{pmatrix}_{x=0} = RT_B \begin{pmatrix} \mathbb{E}^{+}_{By} \\ \mathbb{H}^{+}_{Bz} \\ \mathbb{E}^{-}_{By} \\ \mathbb{H}^{-}_{Bz} \end{pmatrix}_{x=-L_B}. \quad \text{(A17)}$$

At $x = L$,

$$\begin{pmatrix} E^{+}_{By} + E^{-}_{By} \\ H^{+}_{Bz} + H^{-}_{Bz} \end{pmatrix}_{x=L} = \begin{pmatrix} E^{+}_{Gy} + E^{-}_{Gy} \\ H^{+}_{Gz} + H^{-}_{Gz} \end{pmatrix}_{x=L}; \quad \text{(A18)}$$

i.e.,

$$\begin{pmatrix} f^{+}_{B}(z) & 0 & f^{-}_{B}(z) & 0 \\ 0 & f^{+}_{B}(z) & 0 & f^{-}_{B}(z) \end{pmatrix} \begin{pmatrix} \mathbb{E}^{+}_{By} \\ \mathbb{H}^{+}_{Bz} \\ \mathbb{E}^{-}_{By} \\ \mathbb{H}^{-}_{Bz} \end{pmatrix}_{x=L} = \begin{pmatrix} f^{+}_{G}(z) & 0 & f^{-}_{G}(z) & 0 \\ 0 & f^{+}_{G}(z) & 0 & f^{-}_{G}(z) \end{pmatrix} \begin{pmatrix} \mathbb{E}^{+}_{Gy} \\ \mathbb{H}^{+}_{Gz} \\ \mathbb{E}^{-}_{Gy} \\ \mathbb{H}^{-}_{Gz} \end{pmatrix}_{x=L}. \quad \text{(A19)}$$

First, we multiply by $\bar{f}^{+}_{B}$ and integrate in z. Second, we multiply by $\bar{f}^{-}_{B}$ and integrate in z to obtain

$$\begin{pmatrix} \mathbb{E}^{+}_{By} \\ \mathbb{H}^{+}_{Bz} \\ \mathbb{E}^{-}_{By} \\ \mathbb{H}^{-}_{Bz} \end{pmatrix}_{x=L} = R^{*} \begin{pmatrix} \mathbb{E}^{+}_{Gy} \\ \mathbb{H}^{+}_{Gz} \\ \mathbb{E}^{-}_{Gy} \\ \mathbb{H}^{-}_{Gz} \end{pmatrix}_{x=L} = R^{*} T_{G} \begin{pmatrix} \mathbb{E}^{+}_{Gy} \\ \mathbb{H}^{+}_{Gz} \\ \mathbb{E}^{-}_{Gy} \\ \mathbb{H}^{-}_{Gz} \end{pmatrix}_{x=0} = R^{*} T_{G} R T_{B} \begin{pmatrix} \mathbb{E}^{+}_{By} \\ \mathbb{H}^{+}_{Bz} \\ \mathbb{E}^{-}_{By} \\ \mathbb{H}^{-}_{Bz} \end{pmatrix}_{x=-L_{B}}. \quad \text{(A20)}$$

Finally,

$$\begin{pmatrix} \mathbb{E}^{+}_{By} \\ \mathbb{H}^{+}_{Bz} \\ \mathbb{E}^{-}_{By} \\ \mathbb{H}^{-}_{Bz} \end{pmatrix}_{x=L+L_{B}} = T_{B} R^{*} T_{G} R T_{B} \begin{pmatrix} \mathbb{E}^{+}_{By} \\ \mathbb{H}^{+}_{Bz} \\ \mathbb{E}^{-}_{By} \\ \mathbb{H}^{-}_{Bz} \end{pmatrix}_{x=-L_{B}}. \quad \text{(A21)}$$

If we take into account the propagation inside the two Bragg gratings, the total transmission matrix is the product of the transmission matrices in the Bragg gratings T_B and the M matrix, containing the propagation in the middle grating plus the interaction on the interfaces between the different gratings:

$$T_{total} = T_{B} R^{*} T_{G} R T_{B}. \quad \text{(A22)}$$

3. Eigenmodes of a CRIGF

The eigenmodes of the system (propagating, evanescent, and leaky) are characterized by their principal property; their field can be factorized in the form of Eq. (A1). Thus,

$$F(x = L_{total}, z) = \chi F(x = 0, z) \quad \text{(A23)}$$

$$\Rightarrow T_{total} F(x = 0, z) = \chi F(x = 0, z); \quad \text{(A24)}$$

i.e., the problem is equivalent to finding eigenvalues and eigenvectors of the transmission matrix. The propagation constants (γ) are then obtained from the relation

$$\gamma = \frac{\ln \chi}{i L_{total}}. \quad \text{(A25)}$$

Although simple, this link presents several traps because the logarithm of the complex exponential is determined within integer times $2\pi/L_{total}$, so that the real part of γ cannot be obtained deterministically.

In order to illustrate the influence of the mode interaction on the interface between the different gratings, in what follows we make several reasonable assumptions:

(1) Symmetrizing the problem by assuming that

$$R^{++} = R^{--} = R_1, R^{-+} = R^{+-} = R_2. \quad \text{(A26)}$$

We shall take these coefficients as real ($R_{1,2} \in Re$).

(2) Neglecting the radiation losses due to the transition effects on the interfaces between the gratings, and higher mode interactions. For this aim we consider the relation

$$R_1^2 + R_2^2 = 1. \quad \text{(A27)}$$

(3) In order to enable analytical results, we further assume that the Bragg gratings act as if localized on the interfaces x = 0 and L through the overlap integrals in R, i.e., considering the eigenvalues of $M = R^{*} T_G R$ in Eq. (A24) instead of T_{total}.

After some tedious nontrivial calculations using Mathematica, the four eigenvalues of M are given by the expression

$$f_{1-4} = \cos(KL)\cos(\Delta L) \pm \xi \pm \frac{1}{2}\sqrt{A - 8\xi\cos(\Delta L)\cos(KL)}, \quad \text{(A28)}$$

with

$$A = -2[\sin^2(K + \Delta)L + \sin^2(K - \Delta)L] + 16\frac{R_2^2(1 - R_2^2)}{K^2 - \Delta^2}[K^2\cos^2(KL) - \Delta^2\cos^2(\Delta L)] \quad \text{(A29)}$$

and

$$\xi = \sqrt{\sin^2(\Delta L)\sin^2(KL) - 4\frac{K^2\sin^2(KL) - \Delta^2\sin^2(\Delta L)}{K^2 - \Delta^2}(R_2^2 - R_2^4)}. \quad \text{(A30)}$$

Neglecting the terms proportional to R_2^4 and to $\Delta^2 R_2^2$ yields

$$\xi \approx \sin(KL)\sqrt{\sin^2(\Delta L) - 4R_2^2}. \quad \text{(A31)}$$

Let us take, for example, one of the eigenvalues

$$f_1 = \cos(KL)\cos(\Delta L) - \xi + \frac{1}{2}\sqrt{A - 8\xi\cos(\Delta L)\cos(KL)}. \quad \text{(A32)}$$

If $R_2 = 0$, then

$$\xi_0 \equiv \xi(R_2 = 0) = \sin(\Delta L)\sin(KL), \quad A - 8\xi\cos(\Delta L)\cos(KL) = -4\sin^2[(K + \Delta)L], \quad \text{(A33)}$$

so that

$$f_1 = e^{i(K+\Delta)L}. \quad \text{(A34)}$$

This indicates that without cross-interaction between the modes with propagation constants $K + \Delta$ and $K - \Delta$, which happens if R_2 vanishes, the proper modes inside the middle waveguide do not change.

In the other limit when $\Delta = 0$ (at the boundary of the forbidden gap),

$$f_1 = e^{iKL}(1 - 2R_2) = e^{i(K+\Delta)L + \ln(1-2R_2)} \approx e^{i\left(K + i2\frac{R_2}{L}\right)L}, \quad \text{(A35)}$$

i.e., the interaction induced by R_2 increases the imaginary part of the propagation constant, thus enlarging the initial gap.

In the more general case, when both Δ and R_2 are non-null, but small, the fact that ξ contains a square root prevents us from directly expanding Eq. (A32) in series of R_2 and Δ

around zero. However, it is possible to expand it in series of R_2 and ξ. The expansion in series in ξ of Eq. (A32) around ξ_0 gives the following approximate expressions:

$$\begin{aligned} f_1 &= e^{i(K+\Delta)L}\left[1 - i\sin(\Delta L) + i\sqrt{\sin^2(\Delta L) - 4R_2^2}\right] \\ &= e^{i(K+\Delta)L + \ln\left[1 - i\sin(\Delta L) + i\sqrt{\sin^2(\Delta L) - 4R_2^2}\right]} \\ &\approx e^{i(K+\Delta)L - i\Delta L + iL\sqrt{\Delta^2 - (2R_2/L)^2}} = e^{i\left(K + \sqrt{\Delta^2 - (2R_2/L)^2}\right)L}. \end{aligned} \tag{A36}$$

In the particular cases of $R_2 = 0$ or $\Delta = 0$, we obtain Eqs. (A34) or (A35). Let us recall that

$$\Delta^2 = (K - k_g)^2 - \kappa^2, \tag{A37}$$

and thus

$$\sqrt{\Delta^2 - \left(\frac{2R_2}{L}\right)^2} = \sqrt{(K - k_g)^2 - \kappa^2 - \left(\frac{2R_2}{L}\right)^2}. \tag{A38}$$

This means that the interaction between the counter-propagating modes inside the GMRF region (proportional to κ) is increased by $2R_2/L$, as if the intermodal overlap integral (R_2) is distributed over the waveguide length, the factor 2 can be explained as due to the double effect on the borders of the two Bragg reflectors.

The second study concerns the case of strong coupling, i.e., $R_2 \approx R_1$. Another process of tedious calculations shows that the eigenvalues of the system take the simple form

$$\begin{aligned} &e^{ik^+L} + \frac{R_2}{R_1}e^{ik^-L} + i\frac{\Delta^2}{K^2}\sin(KL), \\ &\frac{R_2}{R_1}e^{ik^+L} + e^{ik^-L} + i\frac{\Delta^2}{K^2}\sin(KL), \\ &e^{-ik^+L} + \frac{R_2}{R_1}e^{-ik^-L} - i\frac{\Delta^2}{K^2}\sin(KL), \\ &\frac{R_2}{R_1}e^{-ik^+L} + e^{-ik^-L} - i\frac{\Delta^2}{K^2}\sin(KL). \end{aligned} \tag{A39}$$

Each one constitutes a hybrid wave composed of two original modes having propagation constants $k^{\pm}$ and coupled through R_2. It is interesting to note that the third terms can be neglected practically, so that when $R_2 \approx R_1$, the eigenvalues take even a more simple form. For the first propagation constant, for example, we obtain

$$e^{ik^+L} + e^{ik^-L} = 2e^{iKL}\cos(\Delta L). \tag{A40}$$

The logarithm of the cosine of the complex argument as a function of the wavelength looks like a worn staircase, with the "vertical" segments forming a flat gap in the dispersion curves of the propagation constants.

REFERENCES

1. L. Mashev and E. Popov, "Zero order anomaly of dielectric coated grating," Opt. Commun. **55**, 377–380 (1985).
2. R. Magnusson and S. Wan, "Design of ideal reflection filters using resonant waveguide gratings," OSA Tech. Digest **11**, 256–259 (1994).
3. D. Rosenblatt, A. Sharon, and A. A. Friesem, "Resonant grating waveguide structures," IEEE J. Quantum Electron. **33**, 2038–2059 (1997).
4. A.-L. Fehrembach, K. Chan Shin Yu, A. Monmayrant, P. Arguel, A. Sentenac, and O. Gauthier-Lafaye, "Tunable, polarization independent, narrow-band filtering with one-dimensional crossed resonant gratings," Opt. Lett. **36**, 1662–1664 (2011).
5. E. Popov and B. Bozhkov, "Corrugated waveguides as resonance optical filters-advantages and limitations," J. Opt. Soc. Am. A **18**, 1758–1764 (2001).
6. G. Niederer, H. P. Herzig, J. Shamir, H. Thiele, M. Schnieper, and Z. Christian, "Tunable, oblique incidence resonant grating filter for telecommunications," Appl. Opt. **43**, 1683–1694 (2004).
7. A.-L. Fehrembach, A. Talneau, O. Boyko, F. Lemarchand, and A. Sentenac, "Experimental demonstration of a narrowband, angular tolerant, polarization independent, doubly periodic resonant grating filter," Opt. Lett. **32**, 2269–2271 (2007).
8. A.-L. Fehrembach, F. Lemarchand, A. Talneau, and A. Sentenac, "High *Q* polarization independent guided-mode resonance filter with 'doubly periodic' etched Ta2O5 bidimensional grating," J. Lightwave Technol. **28**, 2037–2044 (2010).
9. A.-L. Fehrembach, O. Gauthier-Lafaye, K. Chan Shin Yu, A. Monmayrant, S. Bonnefont, E. Daran, P. Arguel, F. Lozes-Dupuy, and A. Sentenac, "Measurement and modeling of 2D hexagonal resonant-grating filter performance," J. Opt. Soc. Am. A **27**, 1535–1540 (2010).
10. F. Lemarchand, A. Sentenac, and H. Giovannini, "Increasing the angular tolerance of resonant grating filters with doubly periodic structures," Opt. Lett. **23**, 1149–1151 (1998).
11. I. Evenor, E. Grinvald, F. Lenz, and S. Levit, "Analysis of light scattering off photonic crystal slabs in terms of Feshbach resonances," Eur. Phys. J. D **66**, 231–239 (2012).
12. A.-L. Fehrembach, D. Maystre, and A. Sentenac, "Phenomenological theory of filtering by resonant dielectric gratings," J. Opt. Soc. Am. A **19**, 1136–1145 (2002).
13. P. Paddon and J. F. Young, "Two-dimensional vector-coupled-mode theory for textured planar waveguides," Phys. Rev. B **61**, 2090–2101 (2000).
14. S. Ura, S. Murata, Y. Awatsuji, and K. Kintaka, "Design of resonance grating coupler," Opt. Express **16**, 12207–12213 (2008).
15. Y. Zhou, M. Moewe, J. Kern, M. C. Y. Huang, and C. J. Chang-Hasnain, "Surface-normal emission of a high-*Q* resonator using a subwavelength high-contrast grating," Opt. Express **16**, 17282–17287 (2008).
16. S. Ura, J. Inoue, K. Kintaka, and Y. Awatsuji, "Proposal of small-aperture guided-mode resonance filter," in *International Conference on Transparent Optical Networks* (IEEE, 2011), paper Th.A4.4.
17. X. Buet, E. Daran, D. Belharet, F. Lozes-Dupuy, A. Monmayrant, and O. Gauthier-Lafaye, "High angular tolerance and reflectivity with narrow bandwidth cavity-resonator-integrated guided-mode resonance filter," Opt. Express **20**, 9322–9327 (2012).
18. K. Kintaka, T. Majima, K. Hatanaka, J. Inoue, and S. Ura, "Polarization-independent guided-mode resonance filter with cross-integrated waveguide resonators," Opt. Lett. **37**, 3264–3266 (2012).
19. X. Buet, A. Guelmani, A. Monmayrant, S. Calvez, F. Lozes-Dupuy, and O. Gauthier-Lafaye, "Robust and simplified cat's-eye external-cavity lasers using cavity resonant integrated grating filters," in *International Conference on Transparent Optical Networks* (IEEE, 2013), paper We.B2.2.
20. J. Inoue, T. Ogura, T. Kondo, K. Kintaka, K. Nishio, Y. Awatsuji, and S. Ura, "Reflection characteristics of guided-mode resonance filter combined with bottom mirror," Opt. Lett. **39**, 1893–1896 (2014).
21. L. Li, "Fourier modal method," in *Gratings: Theory and Numeric Applications*, E. Popov, ed., 2nd ed. (revisited) (Aix Marseille Université, CNRS, Centrale Marseille, Institut Fresnel UMR 7249, 2014), Chap. 13.
22. M. G. Moharam and T. K. Gaylord, "Rigorous coupled-wave analysis of dielectric surface-relief gratings," J. Opt. Soc. Am. **72**, 1385–1392 (1982).

23. P. Lalanne and G. Morris, "Highly improved convergence of the coupled-wave method for TM polarization," J. Opt. Soc. Am. A **13**, 779–783 (1996).
24. E. Popov, "Differential method for periodic structures," in *Gratings: Theory and Numeric Applications*, E. Popov, ed., 2nd ed. (revisited) (Aix Marseille Université, CNRS, Centrale Marseille, Institut Fresnel UMR 7249, 2014), Chap. 7.
25. M. Neviere, "The homogeneous problem," in *Electromagnetic Theory of Gratings*, R. Petit, ed. (Springer, 1980), Chap. 5.
26. Q. Cao, Ph. Lalanne, and J.-P. Hugonin, "Stable and efficient Bloch-mode computational method for one-dimensional grating waveguides," J. Opt. Soc. Am. **19**, 335–338 (2002).
27. C. Grenier, D. Iazikov, and T. W. Mossberg, "Lithographically fabricated planar holographic Bragg reflectors," J. Lightwave Technol. **22**, 136–145 (2004).
28. T. W. Mossberg, C. M. Greiner, and D. Iazikov, "Holographic Bragg reflectors, photonic bandgaps and photonic integrated circuits," Opt. Photon. News **15**, 26–33 (2004).